nature chemical biology

ARTICLES

https://doi.org/10.1038/s41589-021-00775-w

Check for updates

The HaloTag as a general scaffold for far-red tunable chemigenetic indicators

Claire Deo[1,2,6], Ahmed S. Abdelfattah[1,6], Hersh K. Bhargava[1,3], Adam J. Berro[1], Natalie Falco[1,4], Helen Farrants[1], Benjamien Moeyaert[1,5], Mariam Chupanova[1], Luke D. Lavis[1,7] ✉ and Eric R. Schreiter[1,7] ✉

Functional imaging using fluorescent indicators has revolutionized biology, but additional sensor scaffolds are needed to access properties such as bright, far-red emission. Here, we introduce a new platform for 'chemigenetic' fluorescent indicators, utilizing the self-labeling HaloTag protein conjugated to environmentally sensitive synthetic fluorophores. We solve a crystal structure of HaloTag bound to a rhodamine dye ligand to guide engineering efforts to modulate the dye environment. We show that fusion of HaloTag with protein sensor domains that undergo conformational changes near the bound dye results in large and rapid changes in fluorescence output. This generalizable approach affords bright, far-red calcium and voltage sensors with highly tunable photophysical and chemical properties, which can reliably detect single action potentials in cultured neurons.

Fluorescent indicators are critical tools for biology, enabling non-invasive measurements of cellular function. In addition to the essential work of optimizing existing indicators to improve brightness and sensitivity, it is also important to explore entirely new scaffolds that can open up underexplored regions of the electromagnetic spectrum and allow new methods to fine-tune sensor properties. Although the fluorescent sensor field began with small-molecule fluorescent dyes, functional imaging in biology rapidly switched to protein-based sensors after the discovery of green fluorescent protein (GFP). After decades of optimization, genetically encoded calcium indicators (GECIs) and genetically encoded voltage indicators (GEVIs) are increasingly being used to monitor cellular activity in living systems[1,2]. The designs of GECIs such as Green Calcium-Modulated Protein (GCaMP)[3,4] and GEVIs such as Accelerated Sensor of Action Potentials (ASAP)[5] consist of a fluorescent protein linked to a sensor domain. In these sensors, the GFP is typically circularly permuted (cp) to place the sensor domain(s) in close proximity to the GFP chromophore, and conformational change in the sensor domain alters the environment around the chromophore, resulting in a fluorescence change (Fig. 1a).

The rapid adoption of protein-based indicators stems from their two key advantages: (1) cell-specific expression and (2) exploitation of evolved molecular recognition motifs found in nature. The palette of fluorescent proteins is limited, however; the most robust genetically encoded sensors are excited with shorter wavelengths (<550 nm), and analogous sensors based on red-shifted fluorescent proteins have proven much more difficult to optimize[6,7]. Given the spectral flexibility and improved photophysical properties of small-molecule fluorophores, it would be advantageous to combine chemical dyes with the genetic targetability and exquisite molecular recognition of proteins. In previous work, we and others developed hybrid small molecule:protein sensors consisting of a chemical sensor tethered to the HaloTag or SNAP-tag, chemically unmasked by enzyme activity, or Förster resonance energy transfer (FRET)-coupled to a fluorescent protein[8–13]. Although these sensor systems allow cell-specific targeting, they rely on chemical sensor moieties that are challenging to synthesize and deliver selectively to cells, especially in complex tissue.

In this Article, we introduce a new general strategy using the self-labeling HaloTag protein[14,15] as a scaffold for hybrid[16,17] small molecule–protein ('chemigenetic') sensors. This straightforward approach involves the replacement of GFP in established sensors with the HaloTag, followed by labeling with fluorogenic rhodamine dyes[18–21]. This yields bright, far-red calcium and voltage sensors with tunable photophysical and chemical properties that are capable of robust reporting of individual action potentials (APs) in single-trial recordings from cultured neurons.

Results

Structure-guided design of the cpHaloTag scaffold. The motivation for this new chemigenetic scaffold stems from the recent development of fluorogenic rhodamine ligands for self-labeling protein tags such as SNAP-tag and HaloTag. We envisioned a system analogous to cpGFP-based sensors where the dye binding site would be proximal to the sensor domain. Changes to protein structure would alter the equilibrium between the colorless, non-fluorescent lactone (L) form of the rhodamine dye and the colored, fluorescent zwitterion (Z; Fig. 1b). This L–Z equilibrium—and therefore the absorption and fluorescence intensity—is strongly dependent on the environment[22]. Although classic rhodamine dyes typically favor the zwitterionic form, other rhodamine analogs such as the far-red Si-rhodamines exist predominantly in the lactone form in aqueous solution[21]. For example, the HaloTag ligand of Janelia Fluor 635 (JF_{635}–HaloTag ligand, **1**; Fig. 1c) shows almost no visible absorption in aqueous solution, but absorbance and fluorescence increases more than 100-fold upon binding to the HaloTag protein (Fig. 1d).

[1]Janelia Research Campus, Howard Hughes Medical Institute, Ashburn, VA, USA. [2]Present address: Cell Biology and Biophysics Unit, European Molecular Biology Laboratory (EMBL), Heidelberg, Germany. [3]Present address: Biophysics Graduate Program, University of California, San Francisco, San Francisco, CA, USA. [4]Present address: Pharmacological Sciences Graduate Program, University of California, Irvine, Irvine, CA, USA. [5]Present address: Department of Cellular and Molecular Medicine, University of Leuven, Leuven, Belgium. [6]These authors contributed equally: Claire Deo, Ahmed S. Abdelfattah. [7]These authors jointly supervised this work: Luke D. Lavis, Eric R. Schreiter. ✉e-mail: lavisl@janelia.hhmi.org; schreitere@janelia.hhmi.org

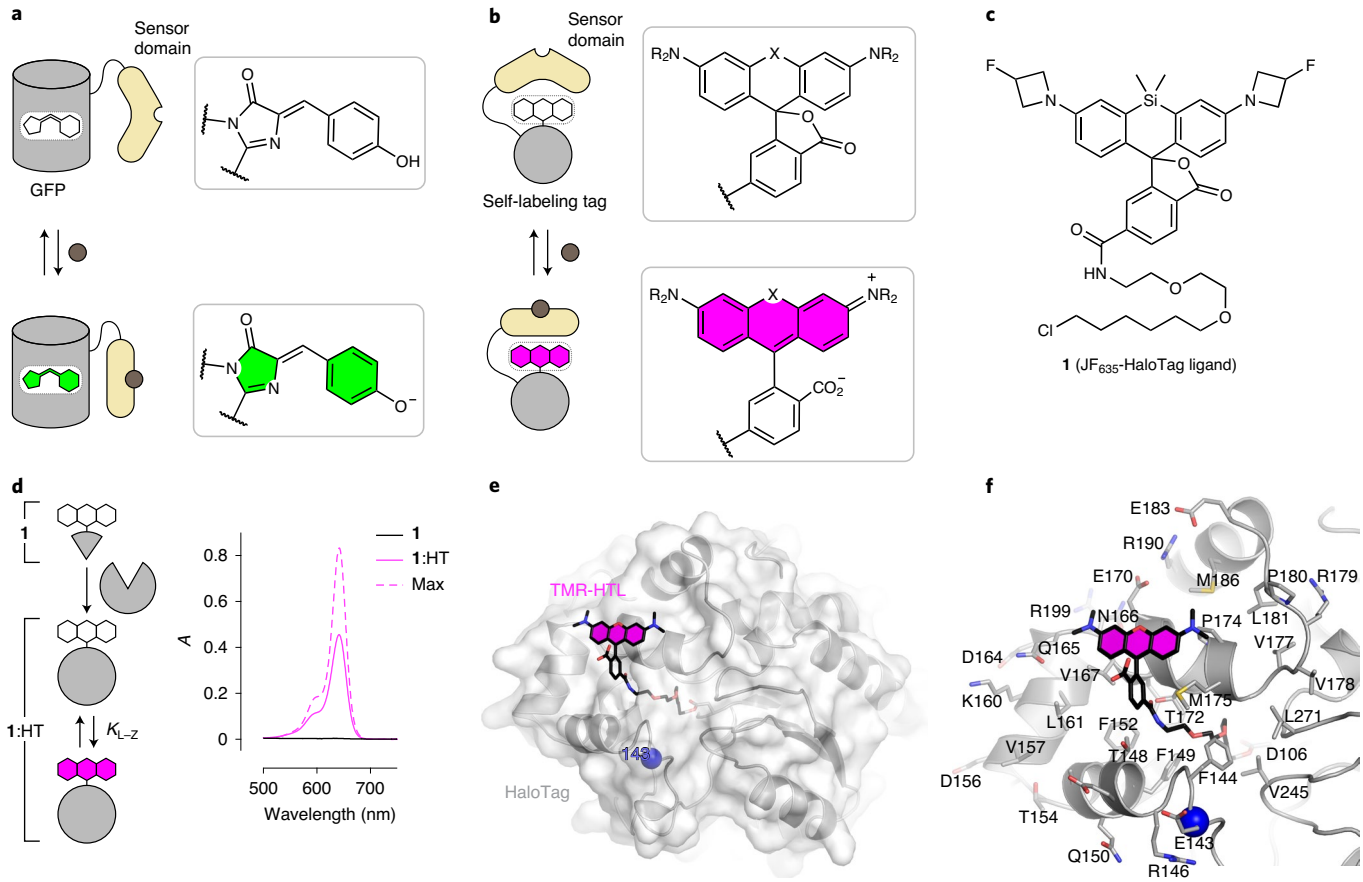

Fig. 1 | Strategy for engineering chemigenetic indicators from HaloTag. a, Non-fluorescent/fluorescent equilibria of the chromophore of GFP in a biosensor. **b**, Non-fluorescent/fluorescent equilibria of the chromophore of a rhodamine dye in a biosensor. **c**, Chemical structure of the JF_{635}-HaloTag ligand (**1**). **d**, Schematic of the reaction of a dye ligand with HaloTag (HT) protein (left) and the absorption spectra of **1** (right) in aqueous solution (black solid line) and bound to HaloTag (magenta solid line). The estimated absorption of the fully zwitterionic form based on experiments in acidic solution is shown as a dashed magenta line. **e**, Crystal structure of HaloTag bound to the tetramethylrhodamine (TMR)-HaloTag ligand. A cartoon and surface representation of the HaloTag protein are shown in gray, the bound TMR–HaloTag ligand is shown by black lines with the xanthene ring system of the rhodamine dye filled in magenta. Position 143 of HaloTag, where it was circularly permuted to create sensors, is shown as a blue sphere. **f**, Closer view of the protein-dye interface in the crystal structure of HaloTag bound to TMR–HaloTag ligand, with amino acid side chains around the dye shown as sticks and labeled.

Further examination of the **1**:HaloTag conjugate revealed that protein binding does not fully shift the equilibrium of the dye to the zwitterionic form; the absorptivity of the JF_{635}–HaloTag conjugate ($\varepsilon = 81{,}000\ M^{-1}\,cm^{-1}$) was lower than the maximal value of free JF_{635} determined in acidic solution ($\varepsilon_{max} = 167{,}000\ M^{-1}\,cm^{-1}$)[21]. This gives an on-protein L–Z equilibrium constant (K_{L-Z}) value of 0.25 for the JF_{635} fluorophore, suggesting that the absorption and fluorescence of this far-red dye could be modulated easily by conformational changes within the protein that modulate its environment (Fig. 1b,d).

To test this hypothesis, we sought cp variants of the HaloTag protein that would allow insertion of sensor domains proximal to the bound fluorophore. To guide our design, we first determined a crystal structure of HaloTag labeled with the HaloTag ligand of tetramethylrhodamine (TMR; Fig. 1e,f and Supplementary Table 1), which was used for the original directed evolution of the HaloTag protein[14,15]. The bound TMR dye appears in the open, zwitterionic form and adopts multiple conformations on the surface of HaloTag (Extended Data Fig. 1). This structure suggests that conformational restrictions imposed by tethering to the protein as well as multiple interaction modes at the protein surface are responsible for the change in fluorophore environment that shifts the L–Z equilibrium of dyes such as **1** towards the fluorescent zwitterionic form upon protein binding. Based on this structure, we identified and tested possible sites for circular permutation to create new N and C termini in close spatial proximity to the bound fluorophore (Extended Data Fig. 2), analogous to the circular permutation of GFP within β-strand seven near its chromophore[23]. We found that circular permutation within the loop around position 143 of HaloTag (cpHaloTag) was well-tolerated and retained functionality.

Development of the HaloCaMP Ca^{2+} sensor. We then tested whether we could swap the cpGFP domain in an established fluorescent sensor with cpHaloTag. We initially focused on calcium indicators due to the established design principles gleaned though the development of several generations of GCaMPs[3,4] and related proteins. Ca^{2+} sensors are also advantageous because they are soluble proteins amenable to in vitro characterization. Based on the GCaMP design, we appended CaM to the new cpHaloTag C terminus and the CaM-binding peptides from myosin light chain kinase (MLCK) or CaM-dependent kinase kinase (CKK) to the N terminus. We gave this new design the name 'HaloCaMP', as it is a direct analog of GCaMP (Fig. 2a and Supplementary Fig. 1a,b). These initial prototypes were subjected to mutagenesis targeting the linkers between cpHaloTag and the peptide (L1) and CaM (L2), which led to two first-generation calcium sensors: HaloCaMP1a, containing the MLCK peptide, and HaloCaMP1b, with the CKK peptide.

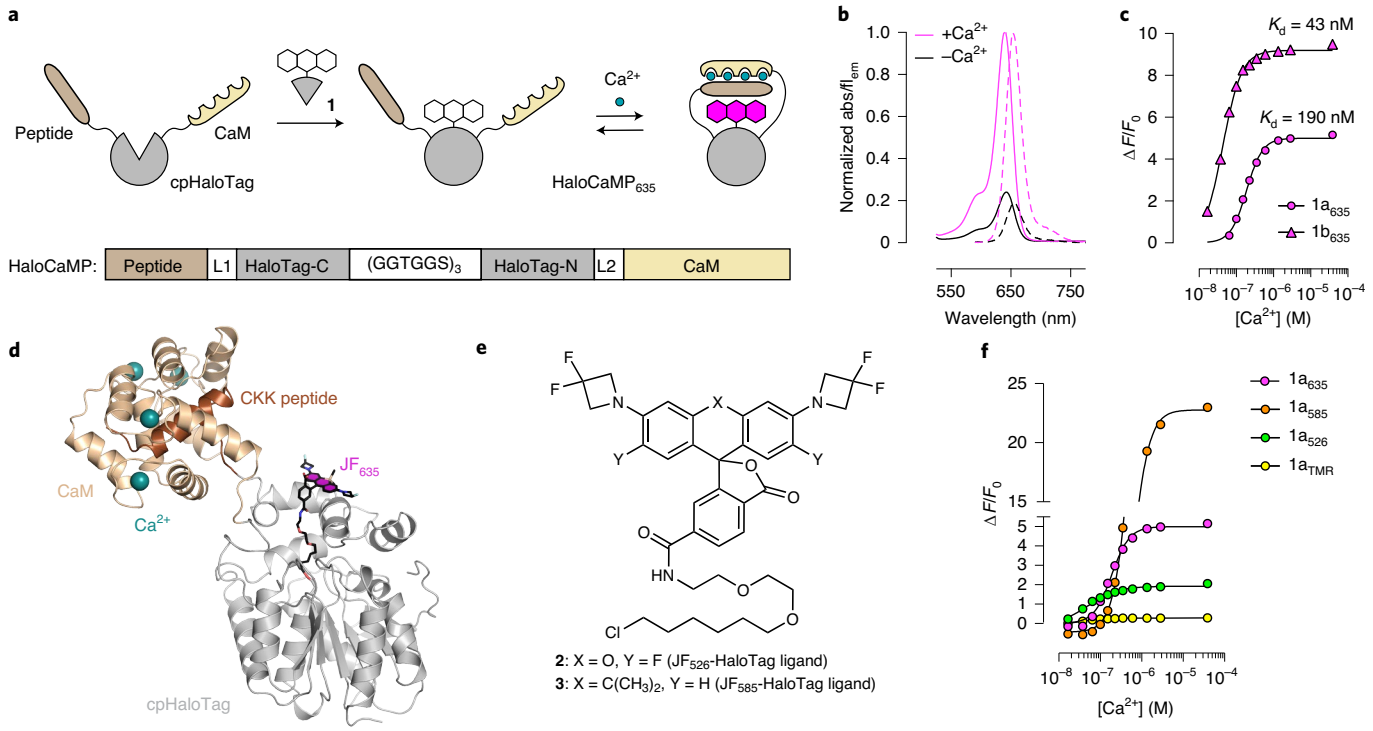

Fig. 2 | HaloCaMP engineering and in vitro characterization. a, Schematic of the chemigenetic calcium indicator HaloCaMP, showing the domain organization (top) and primary structure (bottom). **b**, Normalized absorption (abs, solid lines) and fluorescence (fl_{em}, dashed lines) spectra of HaloCaMP1a$_{635}$. **c**, Calcium titration of HaloCaMP1a$_{635}$ and HaloCaMP1b$_{635}$. Shown are the means of two independent titrations. **d**, Crystal structure of Ca^{2+}-saturated HaloCaMP1b$_{635}$. **e**, Chemical structures of JF$_{526}$–HaloTag ligand (**2**) and JF$_{585}$–HaloTag ligand (**3**). **f**, Calcium titrations of HaloCaMP1a labeled with different fluorophore ligands. Data are presented as the mean of two independent titrations.

We characterized the photo- and bio-physical properties of these new Ca^{2+} sensors after labeling with the JF$_{635}$–HaloTag ligand (**1**; Fig. 2b,c, Supplementary Fig. 2 and Supplementary Table 2). HaloCaMP1a and HaloCaMP1b showed similar fluorescence excitation maxima (λ_{ex}; 640 nm and 642 nm, respectively) and fluorescence emission maxima (λ_{em}; 653 nm and 655 nm, respectively; Fig. 2b). The HaloCaMP1a–JF$_{635}$ sensor showed a relatively large change in fluorescence over baseline ($\Delta F/F_0 = 5.0$) and a high affinity for calcium ($K_d = 190$ nM). At saturating [Ca^{2+}], HaloCaMP1a–JF$_{635}$ exhibited a high extinction coefficient ($\varepsilon_{sat} = 96{,}000\ M^{-1}\,cm^{-1}$) and fluorescence quantum yield ($\Phi_{sat} = 0.78$); these values give a molecular brightness that is 1.7× higher than GCaMP6s ($\varepsilon_{sat} = 70{,}000\ M^{-1}\,cm^{-1}$, $\Phi_{sat} = 0.64$)[24], with a fluorescence spectrum red-shifted by 140 nm. HaloCaMP1b–JF$_{635}$, incorporating the CKK peptide, showed even higher sensitivity and Ca^{2+} affinity ($\Delta F/F_0 = 9.2$, $K_d = 43$ nM) largely stemming from a lower F_0. To gain insight into the mechanism of fluorescence change, we solved a crystal structure of Ca^{2+}-saturated HaloCaMP1b–JF$_{635}$ (Fig. 2d and Supplementary Table 1). The cpHaloTag domain retains the structure of the parent HaloTag, with the zwitterionic fluorophore on the surface of the protein. Interestingly, the Ca^{2+}:CaM:peptide complex does not sit in immediate proximity to the fluorophore, suggesting that the observed fluorescence change results primarily from conformational changes to the linkers.

A useful feature of chemigenetic indicators is the ability to change the small-molecule component to complement protein mutagenesis and allow additional control over sensor properties. We first explored modulating the spectral properties of the sensor system by testing previously described fluorogenic HaloTag ligands based on the yellow-emitting JF$_{526}$ (**2**; $\lambda_{ex}/\lambda_{em} = 526$ nm/550 nm)[25] and orange-emitting JF$_{585}$ (**3**; $\lambda_{ex}/\lambda_{em} = 585$ nm/609 nm; Fig. 2e)[21] with HaloCaMP1a. Both the HaloTag ligands **2** and **3** efficiently labeled HaloCaMP1a and resulted in functional sensors; the JF$_{526}$ conjugate gave $\Delta F/F_0 = 2.0$ and the JF$_{585}$-labeled protein showed a much larger $\Delta F/F_0 = 23.2$ (Fig. 2f). We also tested the standard TMR-based HaloTag ligand bound to HaloCaMP1a and observed no notable Ca^{2+}-dependent fluorescence change (Fig. 2f). This is consistent with our hypothesis that the HaloCaMP sensor functions by shifting dyes from the lactone to the zwitterion form. Dyes that are already largely shifted to the zwitterionic form, such as the TMR fluorophore, are not substantially modulated by the conformational changes in the protein.

Fine-tuning far-red HaloCaMP ligands. After establishing the modularity of HaloCaMP with existing fluorogenic rhodamine dyes, we synthesized a panel of new Si-rhodamine ligands to allow fine-tuning of this far-red sensor scaffold. We previously reported a general method to modulate the K_{L-Z} of the Janelia Fluor dyes by introducing substituents on the 3-position of the azetidine rings[21]. Although we synthesized many different oxygen-containing rhodamine variants using this strategy, we made only a single Si-rhodamine variant—JF$_{635}$—containing the 3-fluoroazetidine motif. We reasoned that other substituted azetidines would yield minor alterations to the K_{L-Z} of Si-rhodamine ligands, and ultimately allow fine-tuning of the sensor properties while retaining far-red excitation and emission. To test this hypothesis, we transformed the Si-fluorescein ditriflate **4** into a set of novel Si-rhodamine HaloTag ligands (**6**–**10**), using a Pd-catalyzed cross-coupling approach (Fig. 3a and Extended Data Fig. 3)[26]. As expected from previous work on rhodamine dyes, the substitution on the azetidine rings elicited only small shifts in λ_{ex} (614–639 nm) and λ_{em} (631–656 nm), with λ_{ex} showing good correlation with the Hammett inductive

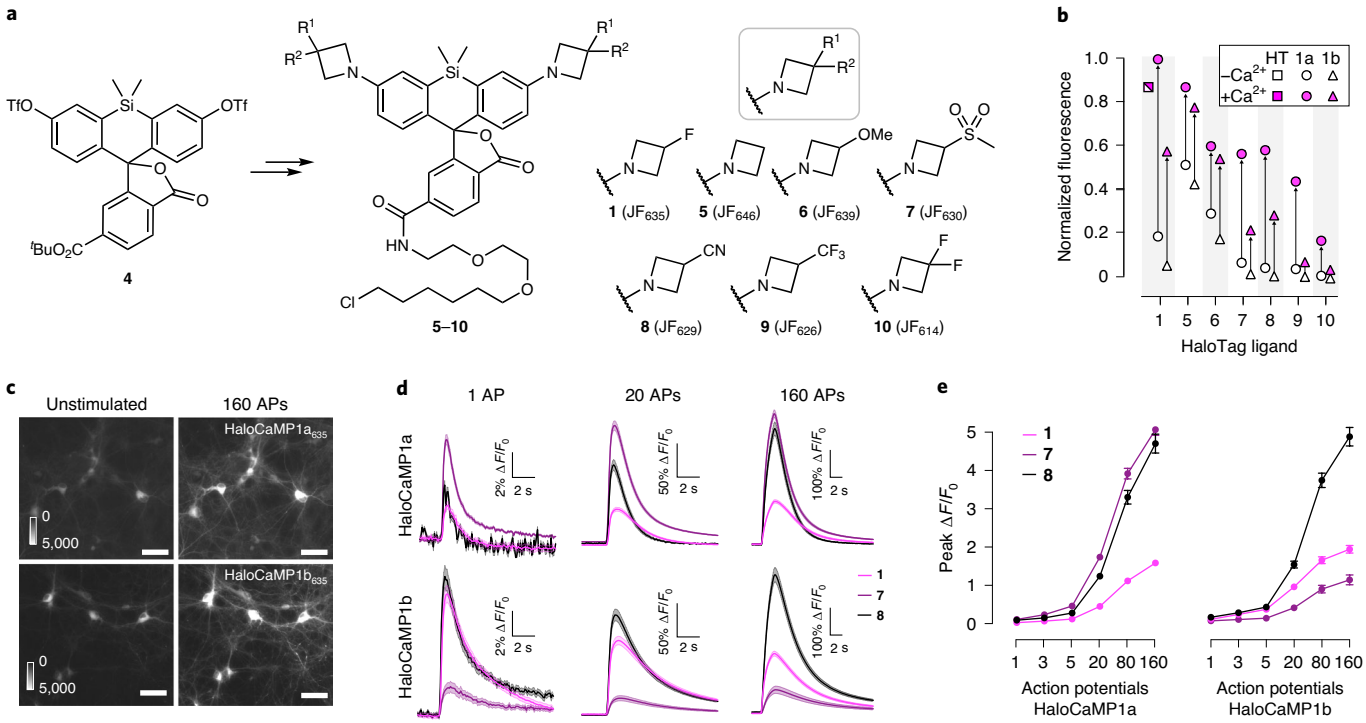

Fig. 3 | Synthesis of Si-rhodamine derivatives and characterization of HaloCaMP in neuron cultures. a, Schematic of the synthetic route to Si-rhodamine derivatives **5**–**10**. **b**, Relative Ca^{2+}-free and Ca^{2+}-saturated fluorescence of HaloTag (HT), HaloCaMP1a and 1b bound to Si-rhodamine HaloTag ligands. Values are normalized to Ca^{2+}-saturated HaloCaMP1a$_{635}$. **c**, Cultured rat hippocampal neurons expressing HaloCaMP1a (top) or 1b (bottom) and labeled with JF$_{635}$–HaloTag ligand (**1**), unstimulated (left) and upon stimulation with 160 APs (right). Scale bars, 50 µm. **d**, Fluorescence response of HaloCaMP1a (top) and 1b (bottom) labeled with Si-rhodamine HaloTag ligands to different numbers of APs at 80 Hz. Data are presented as mean and s.e. for $n = 75$–120 neurons. **e**, Peak $\Delta F/F_0$ as a function of the number of APs. Data are presented as mean and s.e. for $n = 75$ to 120 neurons.

substituent constants (σ_i)[27] for the different azetidine substituents (Extended Data Fig. 4 and Supplementary Tables 3 and 4). Like most other Si-rhodamine derivatives, the free dyes and unbound HaloTag ligands exhibited low extinction coefficients (ε) in aqueous buffer, and binding of the HaloTag ligands to purified HaloTag protein resulted in large increases in absorption and fluorescence (Extended Data Fig. 4e).

We then evaluated the performance of these dyes in the HaloCaMP system. All the Si-rhodamine HaloTag ligands could label HaloCaMP1a and HaloCaMP1b, resulting in functional sensors that showed a fluorescence increase with increasing [Ca^{2+}] (Fig. 3b, Extended Data Fig. 5 and Supplementary Table 5). The sensor properties—$\Delta F/F_0$, K_d and fluorescence intensity—varied substantially over the series of modified dyes, producing a range of indicators with different properties, all based on a single protein. In general, the electron-withdrawing capacity of the azetidine substituents was correlated with $\Delta F/F_0$, decreasing both F_0 and F_{sat}. Ligands based on the unsubstituted azetidine (JF$_{646}$–HaloTag ligand; **5**) and the 3-methoxy variant (JF$_{639}$–HaloTag ligand; **6**) provide high Ca^{2+}-free fluorescence, a useful property for imaging small or sparse features. By contrast, the CF_3-containing JF$_{626}$–HaloTag ligand (**9**) and 3,3-difluoroazetidine JF$_{614}$–HaloTag ligand (**10**) exhibit low F_0 and high sensitivity, a desirable feature for imaging in densely labeled samples. The known 3-fluoro JF$_{635}$–HaloTag ligand (**1**) and the new methylsulfone (JF$_{630}$–HaloTag ligand, **7**) and cyano (JF$_{629}$–HaloTag ligand, **8**) derivatives offer a good compromise between brightness and sensitivity.

Functional imaging using HaloCaMP in cultured neurons. We next tested the ability of our chemigenetic Ca^{2+} indicators to detect neuronal activity. We expressed HaloCaMP in cultured primary rat hippocampal neurons and labeled the proteins with fluorescent dyes, starting with the JF$_{635}$–HaloTag ligand (**1**; Fig. 3c–e and Extended Data Fig. 6). To quantify the fluorescence responses, APs were evoked by electrical stimulation[28]. HaloCaMP1a–JF$_{635}$ and HaloCaMP1b–JF$_{635}$ showed a large fluorescence increase upon field electrode stimulation, and could detect single APs with $\Delta F/F_0$ of 2.3 ± 0.3% and 8.4 ± 0.6%, respectively (Fig. 3d). We then explored fine-tuning of these sensor properties in cells by using different HaloTag ligands. Both the JF$_{630}$–HaloTag ligand (**7**) and JF$_{629}$–HaloTag ligand (**8**) gave bright fluorescence signals in cells with substantial fluorescence increases upon electrical stimulation (Fig. 3d,e and Extended Data Fig. 7). Consistent with the in vitro measurements (Fig. 3b), the JF$_{629}$–HaloTag ligand (**8**) resulted in substantially larger $\Delta F/F_0$ in response to a high-frequency train of APs using the HaloCaMP1a variant. By contrast, JF$_{630}$–HaloTag ligand (**7**) showed higher sensitivity with HaloCaMP1b. The HaloCaMP variants were substantially brighter, faster and more sensitive in neurons than the recently published far-red GECI NIR-GECO1 (Extended Data Fig. 7)[7].

HaloTag-based voltage indicators. Based on our hypothesis, replacement of GFP with HaloTag in fluorescent sensors of other signals should yield functional indicators as well. To test whether HaloTag was indeed 'plug-and-play', we designed two chemigenetic voltage indicators based on similar voltage-sensitive domains (VSDs) but with different topologies. In the first strategy, we followed the design of ASAP[5], which consists of a cpGFP installed in the loop bridging the third (S3) and fourth (S4) transmembrane α-helices of a VSD from *Gallus gallus*. The movement of helix S4 in response to changes in membrane potential modulates the properties of the GFP chromophore, giving rise to a fluorescence change.

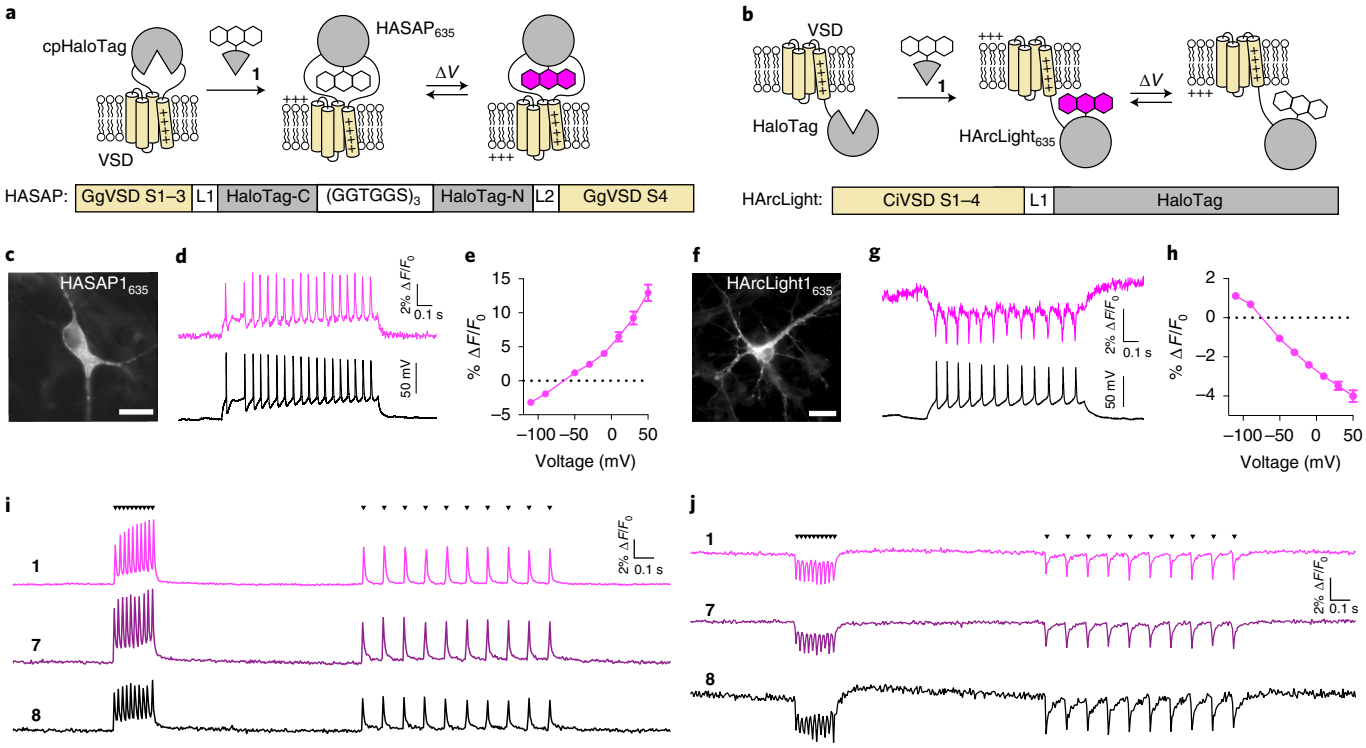

Fig. 4 | Chemigenetic voltage indicators. a, Schematic of the chemigenetic voltage indicator HASAP, showing the domain organization (top) and primary structure (bottom). **b**, Schematic of the chemigenetic voltage indicator HArclight, showing the domain organization (top) and primary structure (bottom). **c**, Fluorescence image of HASAP1 labeled with JF_{635}–HaloTag ligand (**1**) in a rat hippocampal neuron in culture. Scale bar, 20 µm. **d**, Simultaneous fluorescence (magenta) and voltage (black) recordings during current injection from a whole-cell patch electrode for a neuron expressing $HASAP1_{635}$. Data are representative of $n = 4$ neurons. **e**, Fluorescence versus voltage curve for $HASAP1_{635}$ from voltage clamp electrode measurements. **f**, Fluorescence image of HArclight1 labeled with **1** in a rat hippocampal neuron in culture. Scale bar, 20 µm. **g**, Simultaneous fluorescence (magenta) and voltage (black) recordings during current injection from a whole-cell patch electrode for a neuron expressing $HArclight1_{635}$. Data are representative of $n = 5$ neurons. **h**, Fluorescence versus voltage curve for $HArclight1_{635}$ from voltage clamp electrode measurements. **i**,**j**, Fluorescence response of HASAP1 (**i**) and HArclight1 (**j**) in cultured hippocampal neurons labeled with Si-rhodamine HaloTag ligands to a train of field stimuli eliciting 10 APs at 50 Hz followed by 10 APs at 10 Hz. Field stimulus timing is shown with inverted triangles.

We replaced the cpGFP with cpHaloTag (Fig. 4a and Supplementary Fig. 1c), naming this sensor scaffold 'HASAP'. We also explored a different topology based on the GFP-based sensor Arclight[29], which has a non-cpGFP fused to the C terminus of a VSD from *Ciona intestinalis*. In an analogous fashion we prepared a variant called 'HArclight' with HaloTag fused to the S4 helix (Fig. 4b and Supplementary Fig. 1d), similar to previous efforts[30].

The initial HASAP voltage indicator variant could detect APs in single imaging trials from neurons (Extended Data Fig. 8). To improve the HASAP scaffold, we explored mutagenesis of the inter-domain linkers and identified an R467G mutation at the junction of cpHaloTag and helix S4 of the VSD that doubled the voltage sensitivity of the indicator, which we called HASAP1. HASAP1 could be expressed and loaded with dye in cultured neurons (Fig. 4c) and showed fluorescence increases of $9.3 \pm 1\%$ $\Delta F/F_0$ for a voltage step from −70 mV to +30 mV. Current injection during simultaneous whole-cell patch clamp electrophysiology and fluorescence imaging demonstrated that HASAP1 had sufficient sensitivity and response speed to faithfully track membrane potential changes in neurons (Fig. 4d), while voltage clamp measurements were used to quantitate sensitivity (Fig. 4e, Extended Data Fig. 9 and Supplementary Video 1) and response speed (Supplementary Fig. 3 and Supplementary Table 6). HASAP1 was more sensitive than Voltron[19] when both were loaded with **1**. Similarly, HArclight1 functioned in neurons (Fig. 4f–h and Extended Data Fig. 10) with $-3.5 \pm 0.2\%$ $\Delta F/F_0$ fluorescence decreases for a voltage step from −70 mV to +30 mV and appropriate properties for high-speed voltage imaging (Fig. 4g, Supplementary Fig. 4 and Supplementary Table 6). Both voltage sensors could be used with different HaloTag ligands; HASAP showed larger signals with **7** and HArclight showed bigger fluorescence changes with **8** (Fig. 4i,j).

Discussion

The development of new biosensor systems is critical for pushing the frontier of dynamic biological imaging. Here, we have re-engineered the HaloTag protein through circular permutation, transforming this widely used labeling system into a modular scaffold for fluorescent indicators. One of the first hybrid small molecule:protein sensors was developed by Roger Tsien, who exogenously labeled the catalytic and regulatory domains of a kinase enzyme with fluorescein and TMR, respectively, to report enzyme activation as a change in FRET[31]. Although this pioneering hybrid sensor combined synthetic fluorophores and protein sensor domains, most subsequent hybrid sensors rely on tethering or trapping a fully synthetic indicator using exogenous enzymes, thereby requiring the synthesis and delivery of complicated molecules[8–13]. Our chemigenetic approach revisits this combination of protein-based sensor domains with synthetic fluorophores, but allows genetic encoding of the protein portion and uses relatively simple and cell-permeable small-molecule HaloTag ligands. This system proved 'plug-and-play'—new prototype indicators could be designed by simply swapping out GFP domains in established sensors with HaloTag. This work resulted in

bright, far-red calcium and voltage indicators suitable for detecting single APs in neurons. Our approach marries the genetic specificity of protein-based sensors with the superior photophysical properties of small-molecule fluorophores, thereby providing a blueprint for the design of new fluorescent conformational biosensors that overcome limitations of current FP-based sensors.

The linchpin of our chemigenetic indicators is the fluorogenic dye ligand. In recent work, we formulated a general rubric relating the K_{L-Z} value to performance in biological systems[32]. The fluorogenic dye JF_{635}–HaloTag ligand (**1**) and related compounds (**6**–**10**) used in this work have relatively low K_{L-Z} values. These dyes exist primarily in the non-fluorescent lactone form in aqueous solution, which allows substantial modulation by the protein environment when bound to HaloTag, resulting in sensors with large changes in fluorescence intensity. By contrast, ligands that show good bioavailability, such as JF_{525}[19], exhibit intermediate K_{L-Z} values, which aid partitioning in and out of membranes but yield sensors with much smaller fluorescence changes. Development of new fluorogenic dyes that exhibit good bioavailability and/or further engineering of the protein scaffold to modulate existing bioavailable dyes will enable in vivo imaging with this new sensor type. We expect that the continued optimization of these ligands to improve brightness, expand spectral properties and maximize in vivo delivery alongside further protein engineering will generate a large portfolio of sensors useful in a variety of biological contexts.

Online content

Any methods, additional references, Nature Research reporting summaries, source data, extended data, supplementary information, acknowledgements, peer review information; details of author contributions and competing interests; and statements of data and code availability are available at https://doi.org/10.1038/s41589-021-00775-w.

Received: 2 January 2020; Accepted: 19 February 2021;
Published online: 01 April 2021

References

1. Grienberger, C. & Konnerth, A. Imaging calcium in neurons. *Neuron* **73**, 862–885 (2012).
2. Lin, M. Z. & Schnitzer, M. J. Genetically encoded indicators of neuronal activity. *Nat. Neurosci.* **19**, 1142–1153 (2016).
3. Dana, H. et al. High-performance calcium sensors for imaging activity in neuronal populations and microcompartments. *Nat. Methods* **16**, 649–657 (2019).
4. Nakai, J., Ohkura, M. & Imoto, K. A high signal-to-noise Ca^{2+} probe composed of a single green fluorescent protein. *Nat. Biotechnol.* **19**, 137–141 (2001).
5. St-Pierre, F. et al. High-fidelity optical reporting of neuronal electrical activity with an ultrafast fluorescent voltage sensor. *Nat. Neurosci.* **17**, 884–889 (2014).
6. Dana, H. et al. Sensitive red protein calcium indicators for imaging neural activity. *eLife* **5**, e12727 (2016).
7. Qian, Y. et al. A genetically encoded near-infrared fluorescent calcium ion indicator. *Nat. Methods* **16**, 171–174 (2019).
8. Ng, D. N. & Fromherz, P. Genetic targeting of a voltage-sensitive dye by enzymatic activation of phosphonooxymethyl-ammonium derivative. *ACS Chem. Biol.* **6**, 444–451 (2011).
9. Ghitani, N., Bayguinov, P. O., Ma, Y. & Jackson, M. B. Single-trial imaging of spikes and synaptic potentials in single neurons in brain slices with genetically encoded hybrid voltage sensor. *J. Neurophysiol.* **113**, 1249–1259 (2015).
10. Liu, P., Grenier, V., Hong, W., Muller, V. R. & Miller, E. W. Fluorogenic targeting of voltage-sensitive dyes to neurons. *J. Am. Chem. Soc.* **139**, 17334–17340 (2017).
11. Deo, C., Sheu, S. H., Seo, J., Clapham, D. E. & Lavis, L. D. Isomeric tuning yields bright and targetable red Ca^{2+} indicators. *J. Am. Chem. Soc.* **141**, 13734–13738 (2019).
12. Grenier, V., Daws, B. R., Liu, P. & Miller, E. W. Spying on neuronal membrane potential with genetically targetable voltage indicators. *J. Am. Chem. Soc.* **141**, 1349–1358 (2019).
13. Deal, P. E. et al. Covalently tethered rhodamine voltage reporters for high speed functional imaging in brain tissue. *J. Am. Chem. Soc.* **142**, 614–622 (2020).
14. Los, G. V. et al. HaloTag: a novel protein labeling technology for cell imaging and protein analysis. *ACS Chem. Biol.* **3**, 373–382 (2008).
15. Encell, L. P. et al. Development of a dehalogenase-based protein fusion tag capable of rapid, selective and covalent attachment to customizable ligands. *Curr. Chem. Genomics* **6**, 55–71 (2012).
16. Wombacher, R. & Cornish, V. W. Chemical tags: applications in live cell fluorescence imaging. *J. Biophotonics* **4**, 391–402 (2011).
17. Wang, A., Feng, J., Li, Y. & Zou, P. Beyond fluorescent proteins: hybrid and bioluminescent indicators for imaging neural activities. *ACS Chem. Neurosci.* **9**, 639–650 (2018).
18. England, C. G., Luo, H. & Cai, W. HaloTag technology: a versatile platform for biomedical applications. *Bioconjug. Chem.* **26**, 975–986 (2015).
19. Abdelfattah, A. S. et al. Bright and photostable chemigenetic indicators for extended in vivo voltage imaging. *Science* **365**, 699–704 (2019).
20. Grimm, J. B. et al. A general method to improve fluorophores for live-cell and single-molecule microscopy. *Nat. Methods* **12**, 244–250 (2015).
21. Grimm, J. B. et al. A general method to fine-tune fluorophores for live-cell and in vivo imaging. *Nat. Methods* **14**, 987–994 (2017).
22. Lavis, L. D. Teaching old dyes new tricks: biological probes built from fluoresceins and rhodamines. *Annu. Rev. Biochem.* **86**, 825–843 (2017).
23. Baird, G. S., Zacharias, D. A. & Tsien, R. Y. Circular permutation and receptor insertion within green fluorescent proteins. *Proc. Natl Acad. Sci. USA* **96**, 11241–11246 (1999).
24. Chen, T. W. et al. Ultrasensitive fluorescent proteins for imaging neuronal activity. *Nature* **499**, 295–300 (2013).
25. Zheng, Q. et al. Rational design of fluorogenic and spontaneously blinking labels for super-resolution imaging. *ACS Cent. Sci.* **5**, 1602–1613 (2019).
26. Grimm, J. B. & Lavis, L. D. Synthesis of rhodamines from fluoresceins using Pd-catalyzed C–N cross-coupling. *Org. Lett.* **13**, 6354–6357 (2011).
27. Hansch, C., Leo, A. & Taft, R. W. A survey of Hammett substituent constants and resonance and field parameters. *Chem. Rev.* **91**, 165–195 (1991).
28. Wardill, T. J. et al. A neuron-based screening platform for optimizing genetically-encoded calcium indicators. *PLoS ONE* **8**, e77728 (2013).
29. Jin, L. et al. Single action potentials and subthreshold electrical events imaged in neurons with a fluorescent protein voltage probe. *Neuron* **75**, 779–785 (2012).
30. Tsutsui, H., Jinno, Y., Tomita, A. & Okamura, Y. Optically detected structural change in the N-terminal region of the voltage-sensor domain. *Biophys. J.* **105**, 108–115 (2013).
31. Adams, S. R., Harootunian, A. T., Buechler, Y. J., Taylor, S. S. & Tsien, R. Y. Fluorescence ratio imaging of cyclic AMP in single cells. *Nature* **349**, 694–697 (1991).
32. Grimm, J. B. et al. A general method to optimize and functionalize red-shifted rhodamine dyes. *Nat. Methods* **17**, 815–821 (2020).

Methods

Chemical synthesis. Commercial reagents were obtained from reputable suppliers and used as received. All solvents were purchased in septum-sealed bottles under inert atmosphere. Reactions were conducted in round-bottomed flasks or septum-capped crimp-top vials containing Teflon-coated magnetic stir bars. Reactions under inert atmosphere were sealed with septa through which an argon atmosphere was introduced. Heating of reactions was performed with a stirring hotplate equipped with a thermometer to maintain the indicated temperatures.

Reactions were monitored by thin layer chromatography on precoated glass plates (silica gel 60 F_{254}) or by LC-MS (Phenomenex Kinetex 2.1×30 mm, 2.6 µm C18 column; injection of 5–10 µl; 5–98% MeCN/H_2O, linear gradient, with constant 0.1% vol/vol HCO_2H additive; run of 6 min; flow of 0.5 ml min^{-1}; ESI; positive ion mode). The thin layer chromatography chromatograms were visualized by ultraviolet illumination. Reaction products were purified by flash chromatography on an automated purification system using pre-packed silica gel columns or by preparative HPLC (Phenomenex Gemini–NX 30×150 mm, 5 µm C18 column). Analytical HPLC analysis was performed with an Agilent Eclipse XDB 4.6×150 mm, 5 µm C18 column. High-resolution mass spectra were obtained from the High Resolution Mass Spectrometry Facility at the University of Iowa.

NMR spectra were recorded on a 400 MHz spectrometer. Deuterated solvents were used as purchased. ^1H and ^{13}C chemical shifts (δ ppm) were referenced to the residual solvent peaks[33], and ^{19}F chemical shifts (δ ppm) were referenced to $CFCl_3$ added to the tube as a standard. Data for ^1H NMR and ^{19}F NMR spectra are reported by chemical shift (δ ppm), multiplicity (s, singlet; d, doublet; t, triplet; q, quartet; p, pentuplet; dd, doublet of doublets; dt, doublet of triplets; m, multiplet; br s, broad signal), coupling constant (Hz) and integration. Data for ^{13}C NMR spectra are reported by chemical shift (δ ppm) with hydrogen multiplicity (C, CH, CH_2, CH_3) obtained from distortionless enhancement by polarization transfer (DEPT) spectra.

Molecular biology. Generally, cloning was performed by restriction enzyme digestion of plasmid backbones, polymerase chain reaction (PCR) amplification of inserted fragments, and isothermal assembly to combine them, followed by Sanger sequencing to verify the DNA sequences. For the preparation of viruses, plasmid DNA was purified by the Janelia Molecular Biology Facility and adeno-associated viruses (AAVs) were prepared by Janelia Virus Services.

Protein expression and purification. T7 Express *Escherichia coli* cells transformed with pRSET plasmid containing HaloTag-EGFP (EGFP, enhanced GFP), HaloCaMP1a-EGFP, HaloCaMP1b-EGFP, HaloTag, HaloCaMP1a or HaloCaMP1b were grown in LB medium containing ampicillin for 48 h at 25 °C with shaking at 200 r.p.m. After centrifugation, cells were lysed by sonication and the lysate was clarified by centrifugation. Purification from lysate was achieved by nickel-affinity chromatography, followed by size exclusion chromatography using a Superdex 200 10/300 GL column (GE Healthcare) at a flow rate of 0.5 ml min^{-1} in 50 mM Tris-HCl, 75 mM NaCl, pH 7.4. Protein concentration was estimated using the extinction coefficient of EGFP (ε_{488} = 55,900 M^{-1} cm^{-1}) or using the extinction coefficient at 280 nm estimated from the protein sequence.

UV–vis and fluorescence spectroscopy. All measurements were taken at ambient temperature (23 ± 2 °C). Fluorescent molecules were prepared as stock solutions in DMSO and diluted such that the DMSO concentration did not exceed 1% vol/vol. Spectroscopy was performed using 1-cm-path-length quartz cuvettes (Starna) or 96-well clear-bottomed plates (Greiner). Absorption measurements were recorded on a Cary Model 100 spectrometer (Varian). Fluorescence measurement spectra were recorded on a Cary Eclipse fluorometer (Varian) or M100 Pro plate reader (Tecan). Data were analyzed and graphs were plotted using Prism (GraphPad). Absolute quantum yields (Φ) were measured using a Quantaurus-QY spectrometer (model C11374) from Hamamatsu. Measurements were carried out using dilute samples ($A < 0.1$) and self-absorption corrections were performed using the instrument software[34]. For Si-rhodamine dyes, measurements were made in 10 mM HEPES pH 7.4. For the corresponding HaloTag ligands, 0.1 mg ml^{-1} 3-((3-cholamidopropyl)dimethylammonio)-1-propanesulfonate (CHAPS) was added to the buffer. For measurements in the presence of HaloTag protein, the dye was incubated with 1.5 equiv. of purified HaloTag protein (100 µM solution in 75 mM NaCl, 50 mM Tris-HCl, pH 7.4) for 2 h at room temperature. For measurements with HaloCaMP protein, the dye was incubated with 1.5 equiv. of purified HaloCaMP protein (100 µM solution in 75 mM NaCl, 50 mM Tris-HCl, pH 7.4) overnight at room temperature; measurements were then made in a commercial EGTA/Ca·EGTA buffer system (Invitrogen) to which 0.1 mg ml^{-1} CHAPS was added.

Calcium titrations. The HaloTag ligands were incubated with 1.5 equiv. of purified HaloCaMP1a or HaloCaMP1b overnight to guarantee complete binding of the dye ligand. Calcium titrations were performed in a commercial EGTA/Ca·EGTA buffer system (Invitrogen) following the associated protocol. Briefly, different proportions of EGTA buffer (30 mM MOPS pH 7.2, 10 mM EGTA, 100 mM KCl) or Ca·EGTA buffer (30 mM MOPS pH 7.2, 10 mM Ca·EGTA, 100 mM KCl) were mixed to give solutions with different free [Ca^{2+}]. Fluorescence emission was measured on a plate reader. For each fluorophore, λ_{ex} and λ_{em} were adjusted to the values determined for the HaloTag-bound fluorophore. All the calcium titrations were performed in duplicate.

Stopped flow kinetics measurements. Purified HaloCaMP1a or 1b was incubated with 1.5 molar equiv. of JF_{635}–HaloTag ligand (1) and labeled overnight at room temperature. The labeled protein samples were diluted to ~1.3 µM in 30 mM MOPS, 100 mM KCl, 100 µM $CaCl_2$, pH 7.2. A Photophysics SX-20 Stopped-flow device was used to rapidly mix the labeled protein with a solution of 30 mM MOPS, 100 mM KCl, 10 mM EGTA, pH 7.2 in a 1:1 ratio. The JF_{635} label was excited using a light-emitting diode (625 nm), and fluorescence emission was collected through a 665-nm longpass filter. Fluorescence changes over time were fit to the exponential models described in Supplementary Fig. 2. Measurements were made with protein prepared from three independent dye labeling reactions.

Imaging HaloCaMP in primary neuron culture. Primary rat hippocampal neurons were prepared as described previously and infected with AAV viruses. Stock solutions of the different Janelia Fluor ligands were prepared at 1 mM in DMSO. Cultured neurons were incubated with the cell-permeant dyes at 37 °C for 30 min at a final concentration 1 µM before washing twice with imaging buffer containing 145 mM NaCl, 2.5 mM KCl, 10 mM glucose, 10 mM HEPES, pH 7.4, 2 mM $CaCl_2$ and 1 mM $MgCl_2$. Synaptic blockers (10 µM 6-cyano-7-nitroquinoxaline-2,3-dione (CNQX), 10 µM 3-(2-carboxypiperazin-4-yl) propyl-1-phosphonic acid (CPP), 10 µM Gabazine and 1 mM (S)-α-methyl-4-carboxyphenylglycine (MCPG)) were added before imaging. Wide-field imaging was performed on an inverted Nikon Eclipse Ti2 microscope equipped with a Spectra X light engine (Lumencore) with a ×20 objective (NA = 0.75, Nikon) and imaged onto a scientific complementary metal–oxide–semiconductor camera (Hamamatsu ORCA-Flash 4.0). A FITC filter set (475/50 nm (excitation), 540/50 nm (emission), 506LP dichroic mirror (FITC-5050A-000; Semrock)) was used to image GFP. A quad bandpass filter (set no. 89000, Chroma) with 645/30 nm (excitation), 705/72 nm (emission) and 660 nm dichroic mirror (89100bs; Chroma) was used to image all Si-rhodamine derivatives. APs were evoked by field stimulation with a custom-built platinum wire electrode inserted in the medium, controlled by a high-current isolator (A385, World Precision Instruments) set at 90 mA. We stimulated trains of APs from 1 to 160 APs and acquired time-lapse images before, during and after stimulation. Images were processed in ImageJ/Fiji. The Ca^{2+}-dependent fluorescence change was measured for single hand-segmented neurons, on two to four well replicates and multiple fields of view per well.

Field stimulation of HASAP and HArclight in primary neuron culture. A stimulus isolator (A385, World Precision Instruments) with platinum wires was used to deliver field stimuli (50 V, 1 ms) to elicit APs in cultured neurons as described previously[28]. The stimulation was controlled using WaveSurfer and timing was synchronized with fluorescence acquisition using WaveSurfer and a National Instruments PCIe-6353 board. To measure changes of the HASAP or HArcLight fluorescence response to APs over time, neurons expressing these sensors were labeled with the different Janelia Fluor HaloTag ligands and imaged with a ×40 objective at 400 Hz using the same imaging set-up as described for HaloCaMP. We applied field electrode stimulations to induce a train of 10 single APs at 50 Hz, followed by a train of 10 APs at 10 Hz. Images were processed in ImageJ. Voltage-dependent fluorescence changes were measured for hand-segmented neurons, on three well replicates and multiple fields of view per well.

Electrophysiology of HASAP and HArclight in primary neuron culture. Filamented glass micropipettes (Sutter Instruments) were pulled to a tip resistance of 4–6 MΩ. Pipettes were positioned with an MPC200 manipulator (Sutter Instruments). Whole-cell voltage clamp and current clamp recordings were acquired using an EPC800 amplifier (HEKA), filtered at 10 kHz with the internal Bessel filter, and digitized using a National Instruments PCIe-6353 acquisition board at 20 kHz. Data were acquired from cells with access resistance of <25 MΩ. WaveSurfer software was used to generate the various analog and digital waveforms to control the amplifier, camera and light source, and to record voltage and current traces. All electrophysiology measurements were performed in imaging buffer (145 mM NaCl, 2.5 mM KCl, 10 mM glucose, 10 mM HEPES, pH 7.4, 2 mM $CaCl_2$, 1 mM $MgCl_2$, adjusted to 310 mOsm with sucrose). Internal solution for current clamp recordings contained the following: 130 mM potassium methanesulfonate, 10 mM HEPES, 5 mM NaCl, 1 mM $MgCl_2$, 1 mM Mg-ATP, 0.4 mM Na-GTP, 14 mM Tris-phosphocreatine, adjusted to pH 7.3 with KOH, and adjusted to 300 mOsm with sucrose. To generate APs, current was injected (20–200 pA for 1–2 s) and the voltage was monitored. For voltage clamp experiments, the internal pipette solution contained the following: 115 mM cesium methanesulfonate, 10 mM HEPES, 5 mM NaF, 10 mM EGTA, 15 mM CsCl, 3.5 mM Mg-ATP, 3 mM QX-314, adjusted to pH 7.3 with CsOH, and adjusted to 300 mOsm with sucrose. Tetrodotoxin (TTX) (500 nM) was added to the imaging buffer to block sodium channels, synaptic blockers (10 µM CNQX, 10 µM CPP, 10 µM Gabazine and 1 mM MCPG) were added to block ionotropic glutamate, gamma aminobutyric acid (GABA), and metabotropic glutamate receptors. To obtain fluorescence versus voltage curves, cells were held at a potential of −70 mV at the start of each step

and then 1-s voltage steps were applied to step the potential from −110 mV to +50 mV in increments of 20 mV. Fluorescence images were acquired at 400 Hz using the same imaging set-up as described for HaloCaMP above. For determining the response speed of indicators, fluorescence images were acquired at 1,200 Hz in response to a potential step of 100 mV (from −70 mV to +30 mV). Traces were fit to a double exponential function using MATLAB. All recordings were carried out at room temperature.

Crystallography. For crystallization, purified HaloTag or HaloCaMP1b was incubated with 3 equiv. of TMR–HaloTag ligand or JF_{635}–HaloTag ligand (1) for ≥5 h and subsequently purified by size exclusion chromatography in 75 mM NaCl, 50 mM Tris-HCl, pH 7.4 to remove unbound ligand. Crystallization was carried out at ambient temperature (23 ± 2 °C) and crystals were grown using the hanging-drop vapor diffusion method in 24-well plates. HaloTag–TMR (10 mg ml^{-1}) was crystallized by mixing with a precipitant solution of 0.2 M $MgCl_2$, 0.1 M Tris pH 8.5, 20% PEG 8000. HaloCaMP1b$_{635}$ (12 mg ml^{-1}) crystallized 10 days after mixing with a precipitant solution consisting of 30% (vol/vol) PEG 200, 100 mM MES/NaOH pH 6.0 and 5% (wt/vol) PEG 3000 using a 4 µl of protein solution to 1.5 µl precipitant drop ratio. Magenta-colored crystals of HaloTag–TMR were cryoprotected by a quick soak in precipitant solution containing 30% glycerol. Blue HaloCaMP1b$_{635}$ crystals were plunged into liquid nitrogen for storage and transport. X-ray diffraction data for HaloTag–TMR and HaloCaMP1b$_{635}$ were collected at beamlines 24-ID-C at the Advanced Photon Source and 8.2.1 at the Advanced Light Source, respectively, at a wavelength of 1 Å and temperature of 100 K under a cold nitrogen stream. Diffraction data were integrated using iMosflm[35] and scaled using Scala from within the CCP4 suite[36]. Structures were solved by molecular replacement using Phaser[37] with prior structures of HaloTag and calmodulin complexes as search models. Iterative cycles of refinement in Refmac[38] and model rebuilding/adjustment in Coot[39] led to the models described in Supplementary Table 1. The refined HaloTag-TMR and HaloCaMP1b$_{635}$ structures exhibited good model geometry with 96.6/94.7% of residues in the favored regions of the Ramachandran plot and 0/1.4% in disallowed regions, respectively.

Reporting Summary. Further information on research design is available in the Nature Research Reporting Summary linked to this Article.

Data availability

Plasmids have been deposited at Addgene (www.addgene.org) as follows: pAAV-synapsin-HaloCaMP1a (plasmid 138327), pAAV-synapsin-HaloCaMP1b (plasmid 138328), pCAG-HASAP1 (plasmid 138325) and pCAG-HArcLight1 (plasmid 138326). Crystal structures of HaloTag–TMR and HaloCaMP1b$_{635}$ have been deposited at the Protein Data Bank (www.rcsb.org) with accession codes 6U32 and 6U2M, respectively. Source data from experiments in this study are available from the authors upon reasonable request. Source data are provided with this paper.

References

33. Gottlieb, H. E., Kotlyar, V. & Nudelman, A. NMR chemical shifts of common laboratory solvents as trace impurities. *J. Org. Chem.* **62**, 7512–7515 (1997).
34. Suzuki, K. et al. Reevaluation of absolute luminescence quantum yields of standard solutions using a spectrometer with an integrating sphere and a back-thinned CCD detector. *Phys. Chem. Chem. Phys.* **11**, 9850–9860 (2009).
35. Battye, T. G. G., Kontogiannis, L., Johnson, O., Powell, H. R. & Leslie, A. G. W. iMOSFLM: a new graphical interface for diffraction-image processing with MOSFLM. *Acta Crystallogr. D Biol. Crystallogr.* **67**, 271–281 (2011).
36. Winn, M. D. et al. Overview of the CCP4 suite and current developments. *Acta Crystallogr. D Biol. Crystallogr.* **67**, 235–242 (2011).
37. McCoy, A. J. et al. Phaser crystallographic software. *J. Appl. Crystallogr.* **40**, 658–674 (2007).
38. Murshudov, G. N., Vagin, A. A. & Dodson, E. J. Refinement of macromolecular structures by the maximum-likelihood method. *Acta Crystallogr. D Biol. Crystallogr.* **53**, 240–255 (1997).
39. Emsley, P., Lohkamp, B., Scott, W. G. & Cowtan, K. Features and development of Coot. *Acta Crystallogr. D Biol. Crystallogr.* **66**, 486–501 (2010).

Acknowledgements

We acknowledge the Molecular Biology, Cell Culture and Virus Production facilities at Janelia for assistance. This work was supported by the Howard Hughes Medical Institute. B.M. holds a postdoctoral fellowship from the Research Foundation–Flanders (FWO Vlaanderen). The Berkeley Center for Structural Biology is supported in part by the Howard Hughes Medical Institute. The Advanced Light Source is a Department of Energy Office of Science User Facility under contract no. DE-AC02-05CH11231.

Author contributions

C.D., A.S.A., L.D.L. and E.R.S. conceived the project and wrote the manuscript. C.D. contributed organic synthesis, protein engineering, in vitro characterization of proteins, X-ray crystallography and neuron imaging. A.S.A. contributed protein engineering, neuron imaging and electrophysiology. H.K.B. contributed protein engineering, in vitro characterization and neuron imaging. A.J.B. contributed organic synthesis and X-ray crystallography. N.F. contributed organic synthesis. H.F. measured stopped-flow kinetics of purified HaloCaMP. B.M. and M.C. contributed protein engineering and neuron imaging. L.D.L. and E.R.S. directed the project.

Competing interests

C.D., A.S.A., H.K.B., L.D.L. and E.R.S. have filed patent applications on chemigenetic indicators and azetidine-substituted fluorophores.

Additional information

Extended data is available for this paper at https://doi.org/10.1038/s41589-021-00775-w.

Supplementary information The online version contains supplementary material available at https://doi.org/10.1038/s41589-021-00775-w.

Correspondence and requests for materials should be addressed to L.D.L. or E.R.S.

Peer review information *Nature Chemical Biology* thanks Adam Cohen and the other, anonymous, reviewer(s) for their contribution to the peer review of this work.

Reprints and permissions information is available at www.nature.com/reprints.

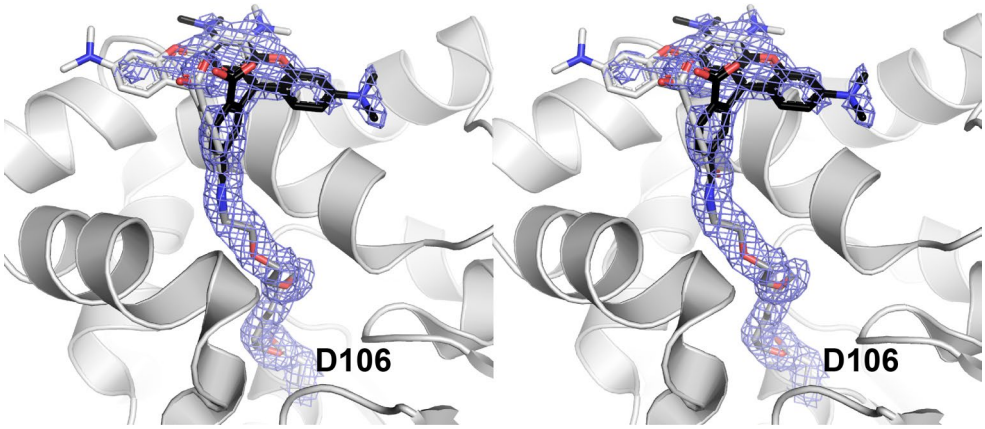

Extended Data Fig. 1 | Multiple conformations of tetramethylrhodamine (TMR) in the HaloTag-TMR structure (PDB 6U32). Stereo view of the region of the bound dye ligand with the HaloTag protein backbone represented as grey cartoon, Asp106 and the bound HaloTag ligand are shown as sticks with grey carbon atoms, and the TMR dye is modeled in two conformations, represented as sticks with black or white carbon atoms. The TMR conformation with black carbon atoms is the one represented in Fig. 1e,f. The $2f_o$-f_c electron density map for the bound dye ligand is shown as purple mesh, contoured at 0.8σ. Although the electron density is strong and continuous for the HaloTag ligand, density for the dye moiety is weaker and broken, suggesting conformational heterogeneity.

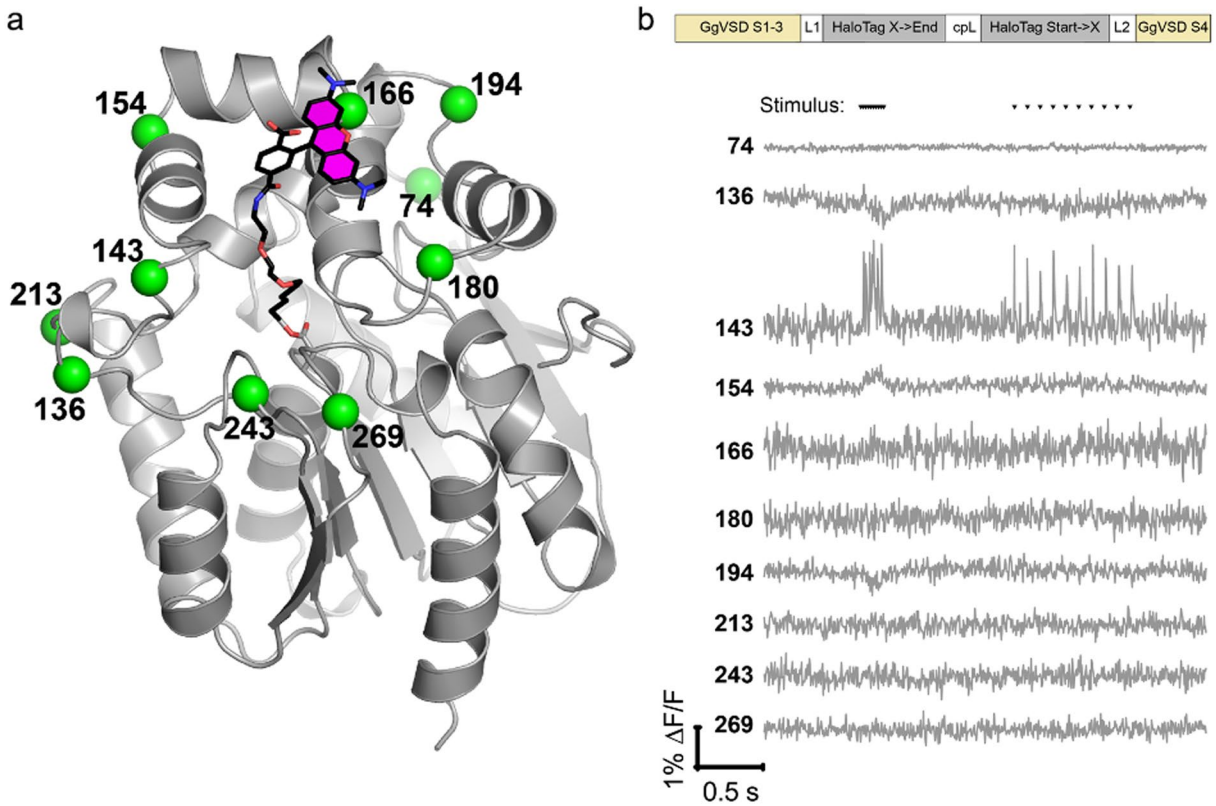

Extended Data Fig. 2 | Exploration of circular permutation sites within HaloTag for sensor design. a, Crystal structure of HaloTag (grey cartoon ribbons) bound to TMR–HaloTag ligand (sticks), illustrating circular permutation sites tested as green spheres labeled with the amino acid number. **b**, Schematic of the sensor context for testing HaloTag circular permutations, with cpHaloTag inserted between helices 3 and 4 of a VSD (top), the field stimulus pattern for stimulation of neurons expressing voltage sensors with cpHaloTag variants (middle), and representative fluorescence traces of each voltage sensor variant in stimulated neurons (bottom).

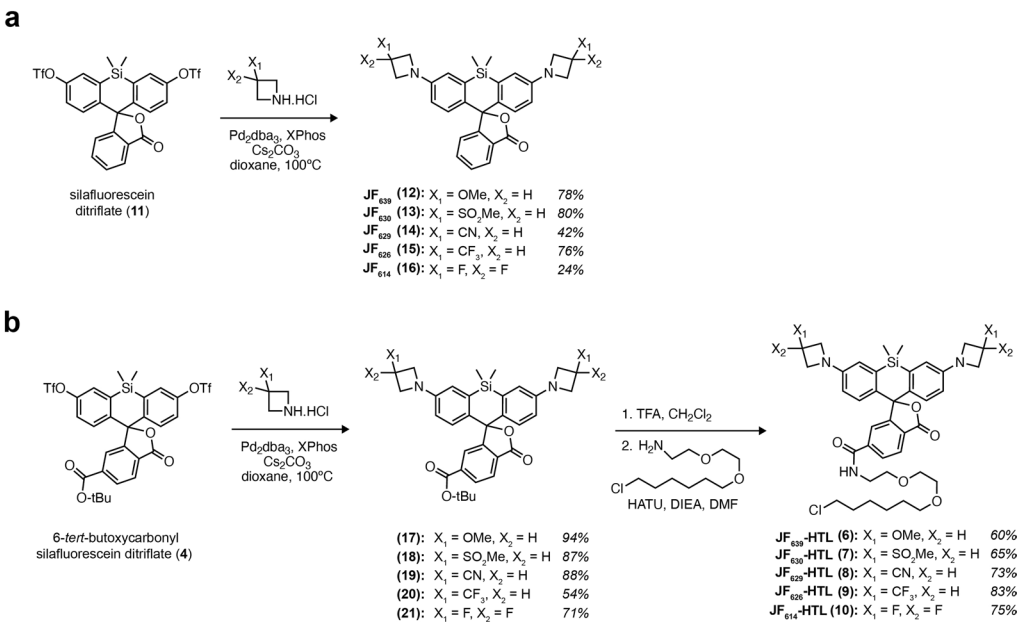

Extended Data Fig. 3 | Synthesis of Si-rhodamine derivatives. Synthesis routes and yields of azetidine-substituted Si-rhodamine derivatives (**a**) and their corresponding HaloTag ligands (**b**).

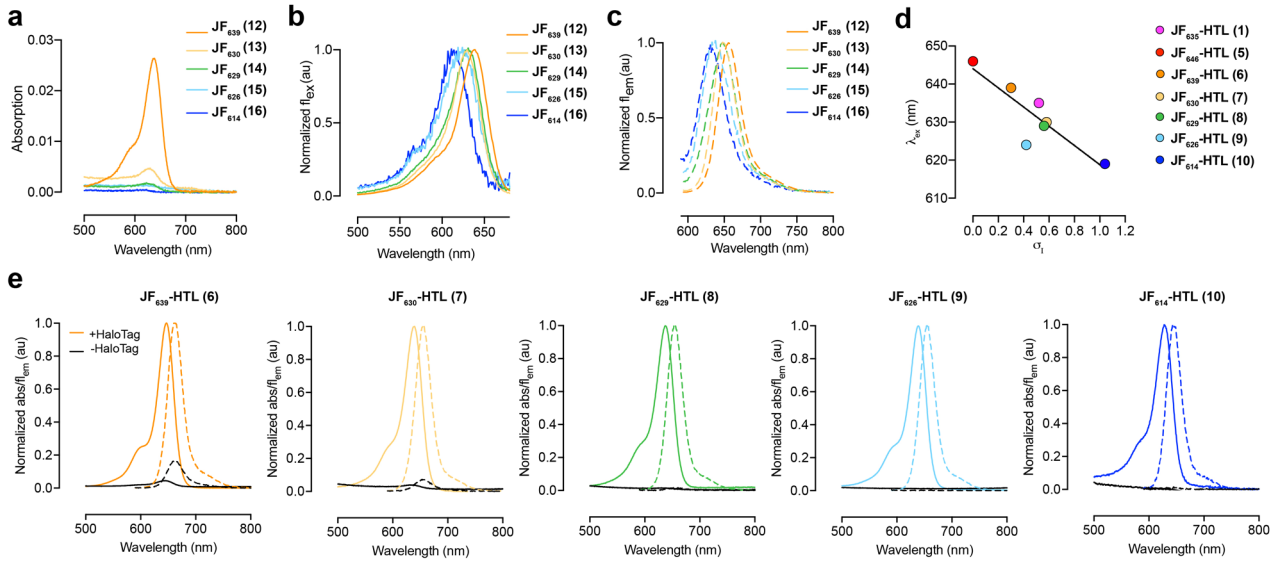

Extended Data Fig. 4 | Spectroscopy of azetidine-substituted Si-rhodamine derivatives. a, Absorption, (**b**) normalized excitation and (**c**) normalized fluorescence emission spectra of novel azetidine-substituted Si-rhodamines. **d**, Correlation of experimental λ_{ex} versus inductive Hammett constants (σ_I) for Si-rhodamines. **e**, Normalized absorption (bold line) and fluorescence (dashed line) spectra of Si-rhodamine HaloTag ligands, in the presence (colored line) or absence (black line) of HaloTag protein. Values were normalized to the HaloTag-bound spectra. All spectra were measured at C = 5 μM in 10 mM HEPES pH = 7.4. In the case of the HaloTag ligands, 0.1 mg.mL^{-1} CHAPS was added to the buffer.

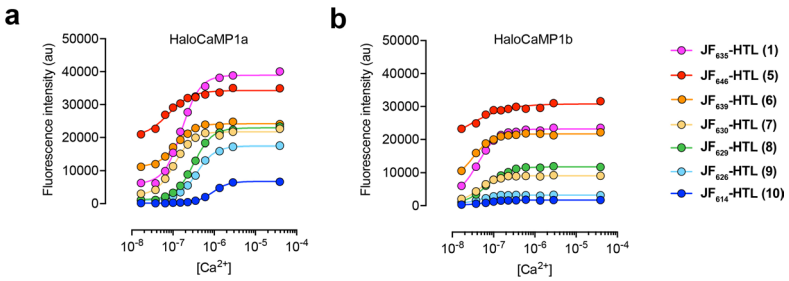

Extended Data Fig. 5 | Calcium titrations. Solution calcium titration curves for purified HaloCaMP1a (**a**) and HaloCaMP1b (**b**) labeled with Si-rhodamine ligands.

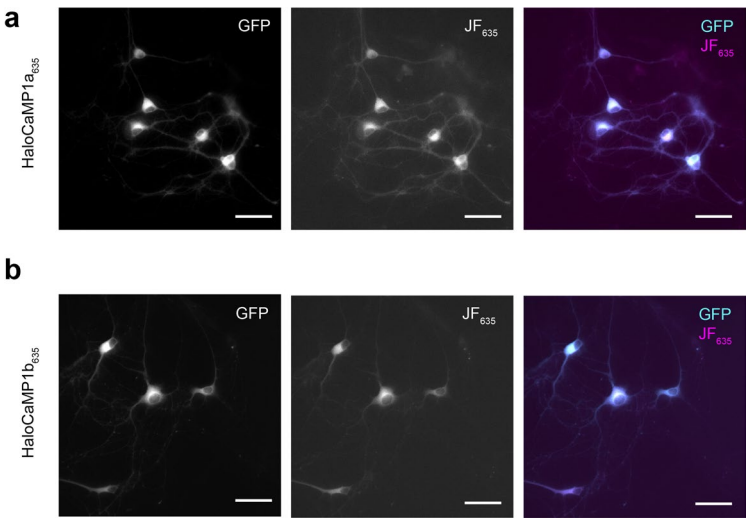

Extended Data Fig. 6 | Labeling of HaloCaMP in neuron cultures. Cultured hippocampal neurons expressing HaloCaMP1a-GFP (**a**) or HaloCaMP1b-GFP labeled with with JF_{635}-HTL (1 μM, 30 min). GFP channel (left panel), JF_{635} channel (middle panel) and merge (right panel); scale bars: 50 μm.

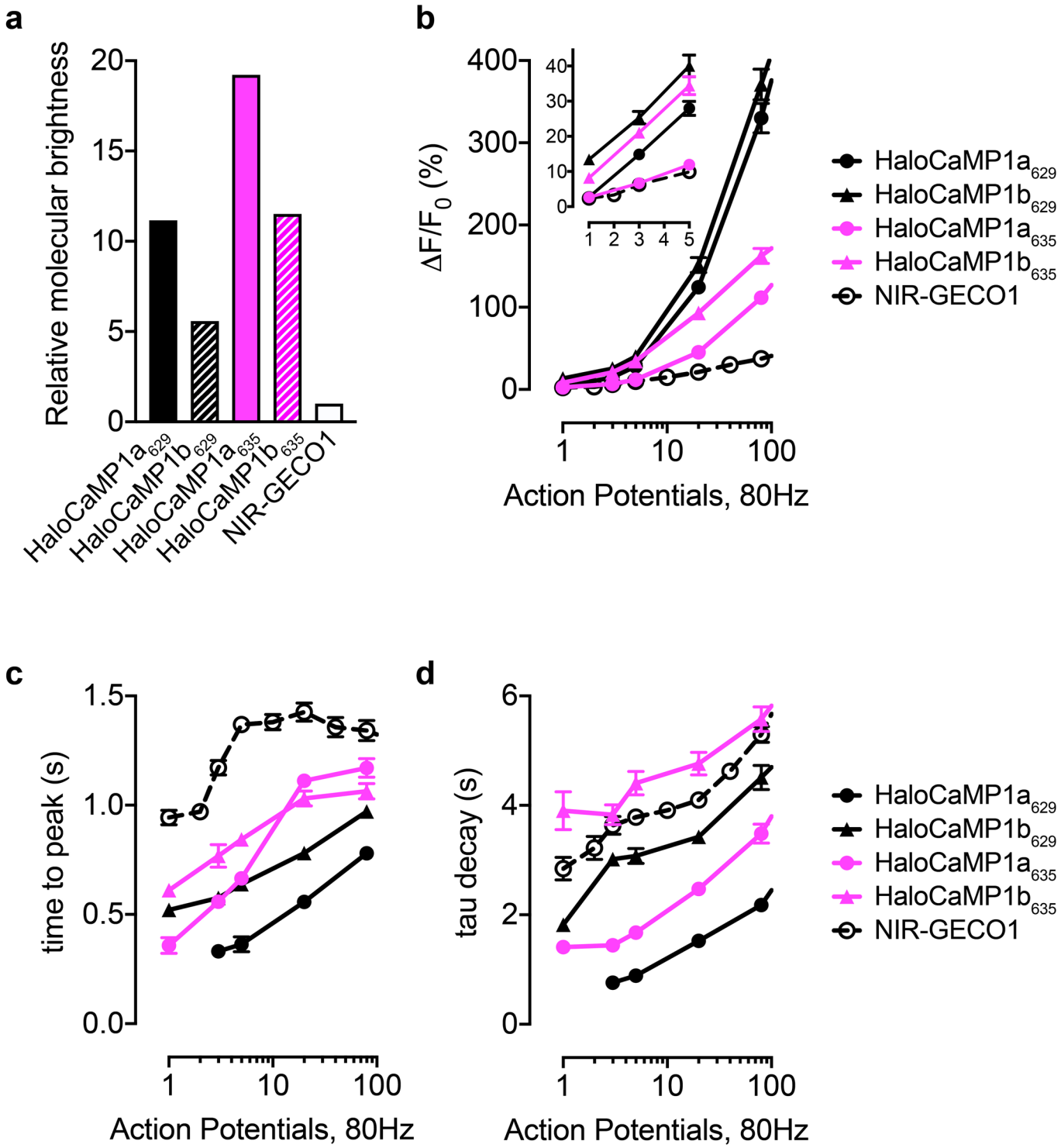

Extended Data Fig. 7 | Comparison of HaloCaMP with NIR-GECO1. a, Comparison of the relative fluorescence brightness (product of quantum yield and extinction coefficient) measured in purified protein solutions. **b**-**d**, Measurements in primary neuron cultures with field stimulation-driven action potentials of (**b**) maximum $\Delta F/F_0$ (**c**) fluorescence rise time, and (**d**) fluorescence decay time.

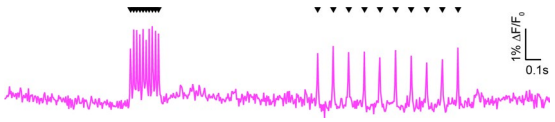

Extended Data Fig. 8 | Fluorescence response in neuron culture of the initial variant of HASAP loaded with JF_{635}-HTL. Black triangles denote the timing of electrical stimuli from the field electrode. Compare with Fig. 4i after additions of the R467G mutation.

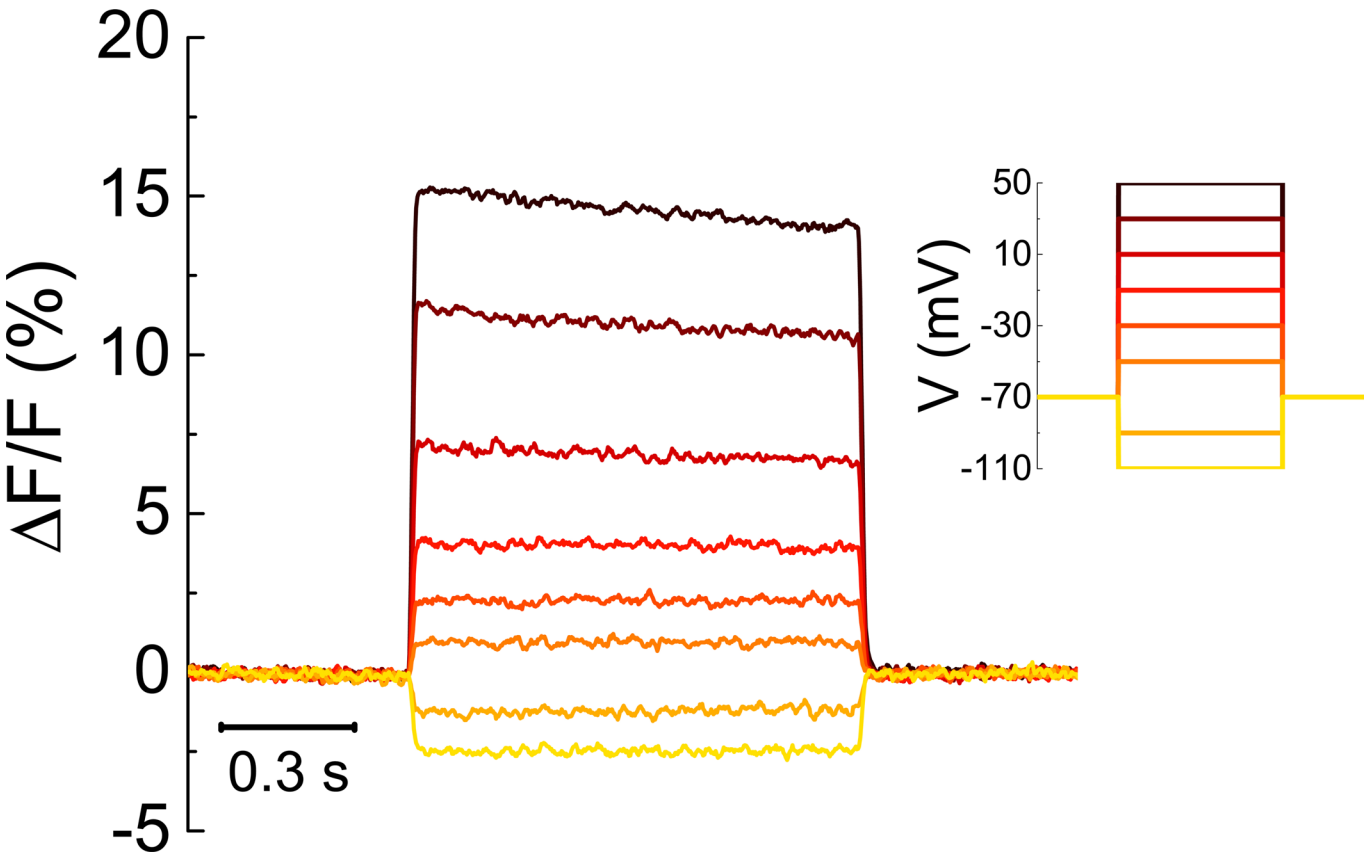

Extended Data Fig. 9 | Fluorescence vs. Voltage for HASAP1$_{635}$. Fluorescence traces of HASAP1$_{635}$ in response to a series of voltage steps (from -110 mV to +50 mV in 20 mV increments). Image acquisition rate = 400 Hz. Representative traces from one cell of N = 8 cells for HASAP1$_{635}$.

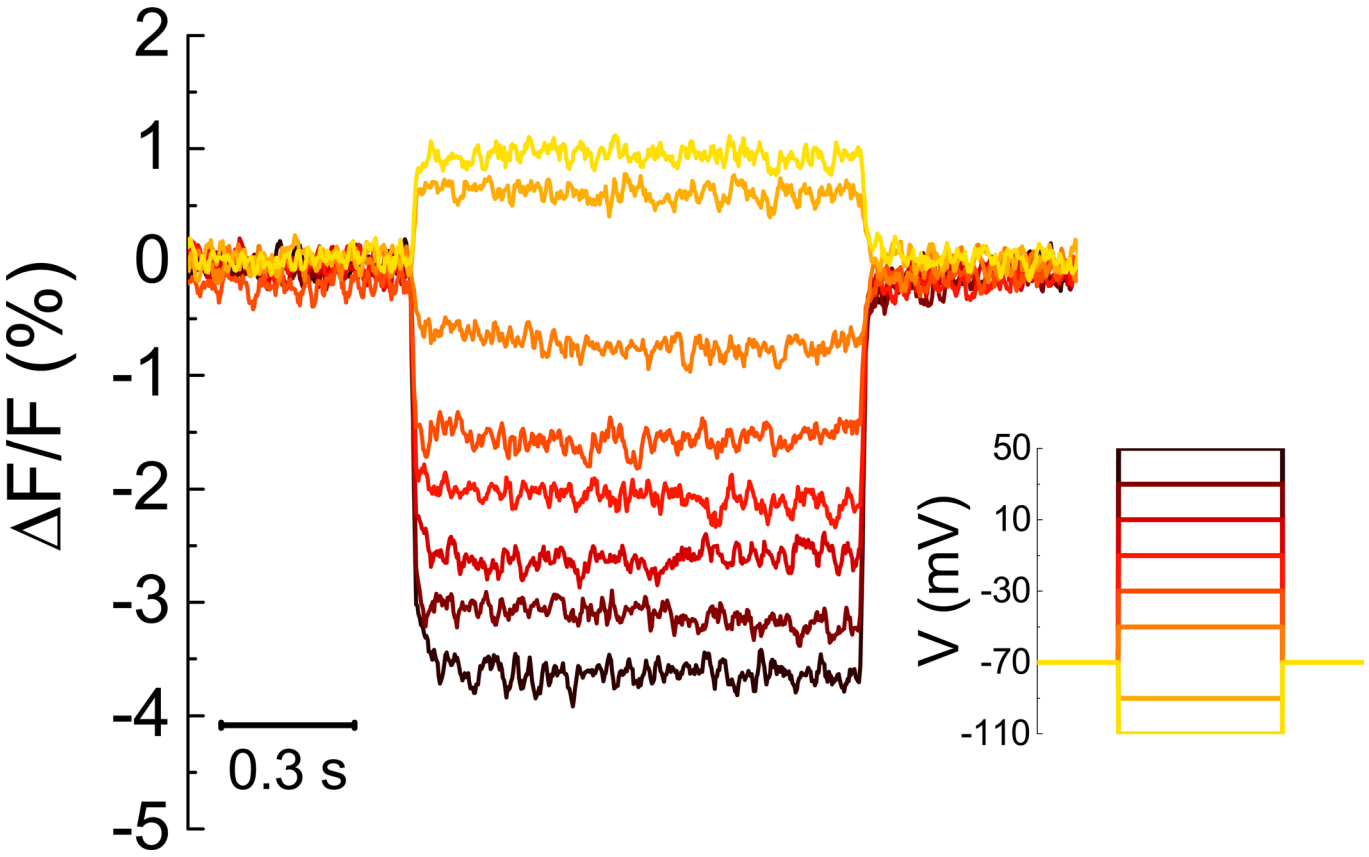

Extended Data Fig. 10 | Fluorescence vs. Voltage for HArcLight1$_{635}$. Fluorescence traces of HArcLight1$_{635}$ in response to a series of voltage steps (from -110 mV to +50 mV in 20 mV increments). Image acquisition rate = 400 Hz. Representative traces from one cell of N = 9 cells.

nature research

Corresponding author(s): Eric Schreiter, Luke Lavis

Last updated by author(s): Feb 1, 2021

Reporting Summary

Nature Research wishes to improve the reproducibility of the work that we publish. This form provides structure for consistency and transparency in reporting. For further information on Nature Research policies, see Authors & Referees and the Editorial Policy Checklist.

Statistics

For all statistical analyses, confirm that the following items are present in the figure legend, table legend, main text, or Methods section.

n/a	Confirmed	
☐	☒	The exact sample size (*n*) for each experimental group/condition, given as a discrete number and unit of measurement
☐	☒	A statement on whether measurements were taken from distinct samples or whether the same sample was measured repeatedly
☐	☒	The statistical test(s) used AND whether they are one- or two-sided *Only common tests should be described solely by name; describe more complex techniques in the Methods section.*
☒	☐	A description of all covariates tested
☒	☐	A description of any assumptions or corrections, such as tests of normality and adjustment for multiple comparisons
☐	☒	A full description of the statistical parameters including central tendency (e.g. means) or other basic estimates (e.g. regression coefficient) AND variation (e.g. standard deviation) or associated estimates of uncertainty (e.g. confidence intervals)
☐	☒	For null hypothesis testing, the test statistic (e.g. *F*, *t*, *r*) with confidence intervals, effect sizes, degrees of freedom and *P* value noted *Give P values as exact values whenever suitable.*
☒	☐	For Bayesian analysis, information on the choice of priors and Markov chain Monte Carlo settings
☒	☐	For hierarchical and complex designs, identification of the appropriate level for tests and full reporting of outcomes
☒	☐	Estimates of effect sizes (e.g. Cohen's *d*, Pearson's *r*), indicating how they were calculated

Our web collection on statistics for biologists contains articles on many of the points above.

Software and code

Policy information about availability of computer code

Data collection	Microsoft Excel for acquisition of fluorescence plate reader data. Nikon Elements and Zeiss ZEN for image acquisition. WaveSurfer (implemented in Matlab) for acquisition of electrophysiology recordings.
Data analysis	Prism 8.2.1 (Graphpad) for curve fitting and statistical tests. FIJI for quantification from of fluorescence images.

For manuscripts utilizing custom algorithms or software that are central to the research but not yet described in published literature, software must be made available to editors/reviewers. We strongly encourage code deposition in a community repository (e.g. GitHub). See the Nature Research guidelines for submitting code & software for further information.

Data

Policy information about availability of data

All manuscripts must include a data availability statement. This statement should provide the following information, where applicable:

- Accession codes, unique identifiers, or web links for publicly available datasets
- A list of figures that have associated raw data
- A description of any restrictions on data availability

Provide your data availability statement here.

Field-specific reporting

Please select the one below that is the best fit for your research. If you are not sure, read the appropriate sections before making your selection.

☒ Life sciences ☐ Behavioural & social sciences ☐ Ecological, evolutionary & environmental sciences

Life sciences study design

All studies must disclose on these points even when the disclosure is negative.

Sample size	No specific sample size calculations were performed. Generally, sample size was the maximum possible within reasonable time and resource allocation limits.
Data exclusions	No data excluded from analysis.
Replication	All attempts at replication were successful.
Randomization	Random allocation of transgenes for expression in neuron cultures.
Blinding	No blinding was performed.

Reporting for specific materials, systems and methods

We require information from authors about some types of materials, experimental systems and methods used in many studies. Here, indicate whether each material, system or method listed is relevant to your study. If you are not sure if a list item applies to your research, read the appropriate section before selecting a response.

Materials & experimental systems

n/a	Involved in the study
☒	☐ Antibodies
☒	☐ Eukaryotic cell lines
☒	☐ Palaeontology
☐	☒ Animals and other organisms
☒	☐ Human research participants
☒	☐ Clinical data

Methods

n/a	Involved in the study
☒	☐ ChIP-seq
☒	☐ Flow cytometry
☒	☐ MRI-based neuroimaging

Animals and other organisms

Policy information about studies involving animals; ARRIVE guidelines recommended for reporting animal research

Laboratory animals	Rattus norvegicus (rat), Sprague-Dawley, 0-1 days.
Wild animals	The study did not involve any wild animals.
Field-collected samples	No field collected samples.
Ethics oversight	All procedures involving animals were conducted in accordance with protocols approved by the Howard Hughes Medical Institute (HHMI) Janelia Research Campus Institutional Animal Care and Use Committee and Institutional Biosafety Committee.

Note that full information on the approval of the study protocol must also be provided in the manuscript.